creative commons

COMMONS DEED

저작자표시-비영리-변경금지 2.0 대한민국

이용자는 아래의 조건을 따르는 경우에 한하여 자유롭게

- 이 저작물을 복제, 배포, 전송, 전시, 공연 및 방송할 수 있습니다.

다음과 같은 조건을 따라야 합니다:

저작자표시. 귀하는 원저작자를 표시하여야 합니다.

비영리. 귀하는 이 저작물을 영리 목적으로 이용할 수 없습니다.

변경금지. 귀하는 이 저작물을 개작, 변형 또는 가공할 수 없습니다.

- 귀하는, 이 저작물의 재이용이나 배포의 경우, 이 저작물에 적용된 이용허락조건을 명확하게 나타내어야 합니다.
- 저작권자로부터 별도의 허가를 받으면 이러한 조건들은 적용되지 않습니다.

저작권법에 따른 이용자의 권리는 위의 내용에 의하여 영향을 받지 않습니다.

이것은 이용허락규약(Legal Code)을 이해하기 쉽게 요약한 것입니다.

Disclaimer

dCollection

[UCI]I804:21031-200000604301

Thesis for the Degree of Master of Engineering

Prediction Methodology for Hollow Hybrid Fins and Arrays under Natural Convection

by

Sina Jamilah

Department of Mechanical Design Engineering

The Graduate School

Pukyong National University

February 2022

Prediction Methodology for Hollow Hybrid Fins and Arrays under Natural Convection

자연대류 하의 중공 하이브리드 핀과 배열의예측방법

Advisor: Prof. Kyoung Joon Kim

by

Sina Jamilah

A thesis submitted in partial fulfillment of the requirements
for the degree of

Master of Engineering

In Department of Mechanical Design Engineering, the Graduate School
Pukyong National University

February 2022

Prediction Methodology for Hollow Hybrid Fins and Arrays under Natural Convection

A thesis

by

Sina Jamilah

Approved by:

(Chairman) Yeon-Won Lee

(Member) Changwon Kim

(Member) Kyoung Joon Kim

February 25, 2022

Acknowledgments

I would like to express my deepest gratitude to my advisor, Prof. Kyoung Joon Kim, for the constant guidance and great support so that I can complete this thesis. Thank you for the clear direction when I needed it the most. He patiently encouraged me to go through all the challenging situations during completing my study.

I am so grateful to my parents for their continuous prayers and unconditional love that gives me strength to overcome daily hardship. Big appreciation to my brothers and sister for all the invaluable support, thank you for always being together.

Many thanks to my lab mates at Thermal Management/Eco-Sustainability Laboratory especially Nico S.E., Hyeon Ho Yang, and Wooheon Noh for their friendship, caring, and kindness. I am blessed to have had them through the ups and downs at the college.

Just as importantly, to all my Indonesian friends who cannot be mentioned one by one. That's very kind of them, I had wonderful and memorable experiences during my study. Thanks for everything.

Busan, 2021

Sina Jamilah

Contents

Acknowledgments i

Contents ii

List of Figures iv

List of Tables vi

Nomenclature vii

Abstract ix

I. Introduction 1

1.1 Background and Purpose 1

1.2 Objective and Research Method 3

1.3 Thesis Outline 5

II. Theory 7

2.1 Extended Surface 7

2.2 Natural Convection 15

2.3 Dimensionless Parameters 17

III. Numerical Modelling 22

3.1 Hollow Hybrid Fin 22

3.2 Hollow Hybrid Fin Array 23

3.3 Numerical Modelling 24

3.4 CFD Model of HHF 28

3.5 CFD Model of HHF Array 31

IV. Experimental Validation 34

4.1 Test Rig Setup 34

4.2 Sample Preparation 38

4.3 Measurement Procedure 40

V. Results and Discussions 42

5.1 Simulation Results 42

5.2 Experimental Results 46

5.3 Nusselt Number Correlations 51

VI. Conclusions 57

List of Publications 59

References 60

PUKYONG NATIONAL UNIVERSITY
부경대학교

List of Figures

Figure 1. Energy balance of a pin fin 8

Figure 2. A hollow hybrid fin boundary condition 10

Figure 3. Temperature and velocity profiles of natural convection heat transfer.. 17

Figure 4. Boundary layer of natural convection around the vertical plate 20

Figure 5. A HHF structure 23

Figure 6. A HHF array structure 24

Figure 7. Evaluation of mesh independence of fin array 28

Figure 8. The numerical model and boundary conditions of a HHF 30

Figure 9. The numerical model and boundary conditions of a HHF array 32

Figure 10. Experimental setup for the HHF and the fin array 36

Figure 11. The schematic of the HHF test rig 37

Figure 12. The schematic of the HHF array test rig 37

Figure 13. A hollow hybrid fin sample for experiment 39

Figure 14. (a) Perspective view and (b) top view of a hollow hybrid fin array sample for experiment 39

Figure 15. Temperature distribution of the HHFs 43

Figure 16. Velocity fields of the HHFs 44

Figure 17. Temperature distribution of the HHF arrays 45

Figure 18. Velocity fields of the HHF arrays 46

Figure 19. IR thermography of a HHF 48

Figure 20. Numerical thermal resistance of HHFs as a function of measured thermal resistance 49

Figure 21. Numerical thermal resistance of HHF arrays as a function of measured thermal resistance 50

Figure 22. The predicted Nusselt number correlations of HHFs at (a) low Ra (b) high Ra as a function of numerically-evaluated Nusselt number of HHFs. 53

Figure 23. The predicted Nusselt number correlations of HHF arrays at (a) low Ra (b) medium Ra (c) high Ra as a function of numerically-evaluated Nusselt number of HHF arrays 56

List of Tables

Table 1. Solution methods of numerical calculations..... 27

Table 2. Variations of outer diameter and inner diameter of HHF configurations. 29

Table 3. Summary of computational settings of HHFs 30

Table 4. Summary of fin arrays configurations..... 32

Table 5. Summary of computational settings and solution methods of HHF arrays 33

Table 6. Equipment and components of experimental setup..... 35

Table 7. Dimensions of samples for experiment 38

Table 8. Uncertainty of the HHF and the HHFHS experiments..... 47

Table 9. Temperature measurement of the HHFs 48

Table 10. Empirical constants of Nusselt number correlations of the HHFs 52

Table 11. Empirical constants of Nusselt number correlations of the HHF arrays 55

Nomenclature

A	area [m^2]
C	empirical constant
D	fin diameter [mm]
g	gravity [m/s^2]
H	fin height [mm]
h_c	convective heat transfer coefficient [W/m^2-K]
k	thermal conductivity [W/m-K]
L_c	characteristic length [m]
N	fin number
Nu	Nusselt number
P	pressure [Pa]
q	heat transfer rate [W]
Pr	Prandtl number
Ra	Rayleigh number
R_{th}	thermal resistance [K/W]
S	fin spacing [mm]
T	temperature [°C]
ΔT	temperature difference between the heat sink and the ambient [K]
u	x – velocity [m/s]

v	y – velocity [m/s]
w	z – velocity [m/s]
W	plate fin width [mm]

Greek symbols

α	thermal diffusivity [m^2/s]
β	volumetric thermal expansion coefficient [1/K]
η	efficiency
ν	kinematic viscosity [m^2/s]
ρ	density [kg/m^3]

Subscripts

a	ambient
b	base
F	fin
FA	fin array
i	inner
o	outer
p	perforation
∞	free stream

Superscripts

cor	correlation
num	numerical

Prediction Methodology for Hollow Hybrid Fins and Arrays under Natural Convection

Sina Jamilah

Department of Mechanical Design Engineering, The Graduate School,
Pukyong National University

Abstract

Recently, the need for electronic and photonic devices is increasing rapidly with higher demands such as smaller sizes with high efficiency and reliability while the cost is expected at low prices. Several electronic and photonic systems such as light-emitting diodes (LEDs), outdoor wireless devices, and defense electronics are located in various conditions including remote areas far from power sources and thus need highly energy efficiency. Heat sinks have been commonly used as passive cooling devices considering their robust design and promising price. However, research on optimum heat sink performance is continuously required to achieve effective thermal management in accordance with the growth of the electronic and photonic technology.

In this study, Nusselt number correlations were developed to predict thermal behaviors of hollow hybrid fins (HHFs) and fin arrays under natural convection. The HHF is a hollow pin fin integrated with radially-placed plate fins and having a perforation near the fin base. The HHF array is a staggered array of the HHFs.

The numerical models of the HHF and the HHF array were generated and validated by the measurement, and then wide-ranging thermal data were obtained using the CFD models. Nusselt number correlations for the HHF and the HHF array were generated utilizing the thermal data, obtained by the CFD models, by considering Rayleigh numbers

and the primary geometric parameters such as external diameter, internal diameter, fin spacing, and the height of the HHF.

The results show that the prediction of the correlations agrees well with the CFD calculation with reasonable discrepancy. The average discrepancy values of HHF correlations were 3.0% for low Ra (Ra<40000) and 2.7% for high Ra (Ra>40000). The average discrepancy values of HHF array correlations were 3.5% for Ra <9000, 8% for 9000<Ra<60000, and 2.8% for 60000<Ra <292000.

PUKYONG NATIONAL UNIVERSITY
부경대학교

I. Introduction

1.1 Background and Purpose

The rapid development of electronic and photonic systems demand high efficiency and reliability, while the size and weigh are reduced as well as the cost [1-6]. Electronic and photonic systems such as light-emitting diodes (LEDs), outdoor device electronics, and remote radio transceivers are installed in various conditions including in remote areas and need highly energy efficiency [4-6]. This poses a challenge for thermal management technology in keeping electronic and photonic devices cool. Heat sinks have been widely used as effective thermal managements considering their robustness and cost-effectiveness. Natural convection cooling is the most suitable method for these conditions.

Weight becomes one of critical parameters in heat sink design that requires high performance and limited volume with a low cost production. Several researches have been meticulously conducted on lightweight heat sinks. Sonn and Bar-Cohen optimized cylindrical pin fin to obtain least material for dissipating an amount of heat flux [7]. Bar-Cohen et al. determined a methodology of optimization on polyphenylene sulphide (PPS) polymer heat sink based on least material [8]. Icoz et al. conducted experimental and theoretical investigation of lightweight heat sink materials [9].

Many researches reported that heat sinks performance are affected by their orientation. Sparrow et al. explored orientation effects of natural convection and radiation heat transfer on cylindrical pin fin heat sink [10]. Lee et al. developed cross-cut cylindrical heat sink correlation associated with the effects of orientation [11]. Sertkaya et al. performed experimental research of natural convection cooling on cylindrical fin heat sinks with various orientations [12]. Huang et al. explored the orientation effects on the square pin fin heat sinks under natural convection [13]. Shen et al. conducted the numerical and experimental study of orientation effects on rectangular fin heat sinks with natural convective heat transfer [14].

Recently, researches on optimization of heat sinks have been performed on various geometries of heat sink to achieve high performance of thermal management. Aihara et al. experimentally examined the performance of pin fin arrays with sideward orientation on combined of natural convection and radiation [15]. Elshafei researched on hollow/perforated circular pin fin heat sink [16]. Lee et al. performed multidisciplinary method for optimization of pin fin radial heat sink [17]. Kou et al. analyzed several fin cross-sections of heat sinks theoretically [18].

Our prior studies introduced an innovative structure of lightweight heat sink for natural convection cooling [19, 20]. Considering the manufacturability, the structures of heat sinks were simplified by promoting a solid hybrid fin (SHF) and a hollow hybrid fin (HHF) [21]. The performance of hollow hybrid fins (HHFs) was investigated as a lightweight structure for heat sinks. The results demonstrated that

a hollow hybrid fin heat sink (HHFHS) has a better performance than pin fin heat sink (PFHS) [22, 24, 26]. Orientation effects of the hollow hybrid fin heat sink (HHFHS) was numerically-evaluated and compared with pin fin heat sink (PFHS) and solid hybrid fin heat sink (SHFHS). It was found that HHFHS less orientation dependent than PFHS [23]. Prediction methods were evaluated and developed for natural convection around HHFHSs. The correlations were in good agreements with the numerical results [25]. However, prediction correlations on single HHF and HHF array have not yet been revealed. Therefore, further investigation on HHFs and HHF arrays should be rigorously carried out to predict their thermal behavior.

This study discusses the Nusselt number development for hollow hybrid fins (HHFs) and HHF arrays under natural convection. This paper describes the HHF and the HHF array structures. CFD models are illustrated based on the structures. Then, experimental study is shown to validate the numerical models. Lastly, the development of Nusselt number correlations of the HHFs and the HHF arrays are discussed utilizing broad range of CFD models.

1.2 Objective and Research Method

This thesis aims to develop a prediction methodology of the hollow hybrid fins (HHFs) and fin arrays to investigate their thermal behavior under natural convection. The HHF is a lightweight structure of fin for heat sink used to cool the electronic and photonic devices. The predicted Nusselt number correlations are

determined utilizing wide-range of numerical thermal data. Several actions were taken to achieve this goal as described below.

Firstly, numerical investigation is conducted on various configurations of HHF and HHF array consisting primary geometrical parameters such as external diameter, internal diameter, fin height, and fin spacing. ANSYS software is utilized to generate CFD models of the HHF and array. The mesh is generated using ANSYS ICEM CFD then numerical calculation is performed using ANSYS FLUENT. ANSYS CFD POST is employed to access and analyze the computational results. The numerical thermal data is obtained with several base temperatures on the HHFs and arrays.

Secondly, an experimental test rig is prepared for validation process of CFD models of the HHFs and fin arrays. Equipment and devices such as power supply, PC, thermocouples, data logger, and IR camera are used in this experiment. The HHFs and the fin arrays bases are uniformly heated at certain temperatures using a heater. The insulation layers are installed to avoid heat loss. For validation purposes, the experimentally-evaluated thermal resistance is compared with the numerically-obtained thermal resistance.

Finally, Nusselt number correlations are developed for HHFs and fin arrays. The thermal data from numerical calculation is used to generate the correlations by considering Rayleigh number and main parameters of the HHF and fin array structures.

1.3 Thesis Outline

This thesis outline consists of six (6) chapters of the study. The chapters are introduction, theory, numerical modeling, numerical validation, results and discussion, and conclusions. Every chapter is briefly explained as follow.

Chapter 1: Introduction

The introduction describes background and purpose of this research. Then the objective and research method are explained. Lastly, the thesis outline is provided.

Chapter 2: Theory

This chapter presents the theory of heat transfer from an extended surface and convection heat transfer including the equations and important dimensionless parameters related to the natural convection case.

Chapter 3: Numerical Modeling

This part explains thermal data collection of HHFs and fin arrays using numerical method. The HHF and fin array structures are provided. The governing equations of numerical solution are given, several assumptions are made for calculation, and solution methods are chosen. Various configurations of HHFs and fin arrays for CFD models are presented. Mesh independency is shown to make sure the reliability of the numerical calculation.

Chapter 4: Experimental Validation

The validation process is defined in this chapter. Samples of the HHF and fin array are fabricated and a test rig is prepared with several equipment and measurement devices such as power supply, PC, data logger, thermocouples, and IR camera. The performance of HHFs and fin arrays are observed.

Chapter 5: Results and Discussion

The numerical and experimental results are presented in this chapter. The temperature and velocity fields of numerical solution are shown. The performance of the HHFs and fin arrays are revealed and compared between the measurement and simulation. The Nusselt number correlations of the HHFs and fin arrays are delivered.

Chapter 6: Conclusions

This last chapter summarizes and concludes the research, as well as provides suggestions for further research.

PUKYONG NATIONAL UNIVERSITY
부경대학교

II. Theory

The purpose of this chapter is to provide the description of heat transfer from extended surface and natural convection heat transfer including its important parameters. This part consist of three sections. First, Section 2.1, describes heat transfer equations of extended surface. The second section, 2.2, provides description of natural convection heat transfer. The last section, 2.3, presents several important dimensionless parameters to examine the natural convection flow.

2.1 Extended Surface

An extended surface such as a fin arrangement is commonly used to enhance heat transfer from hot surfaces to surrounding. The heat rate transferred from a fin can be calculated by determining temperature distribution along the fin. In doing so, the energy balance of the fin should be evaluated on an appropriate differential element as displayed on Figure 1. Several assumptions are made to simplify the heat transfer analysis as follow. The calculation based on one-dimensional conduction in longitudinal (x) direction due to the fin is thin. Therefore, the temperature difference in transverse direction (y) within the fin is very small and assumed to be uniform across the fin thickness. The conditions applied to the equations are steady state, no heat generation, constant thermal conductivity, uniform convective heat transfer coefficient over the surface, and negligible

radiation from the surface [33].

Energy Equation

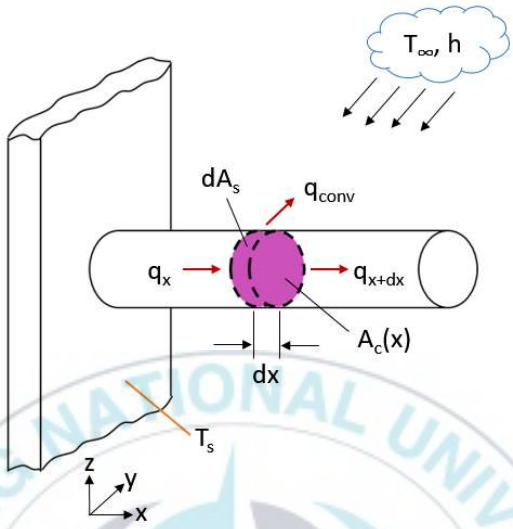

Figure 1. Energy balance of a pin fin

The energy balance of an extended surface is depicted in Figure 1. The conservation of energy for the fin is as follow.

$$q_x = q_{x+dx} + dq_{conv} \tag{1}$$

Using Fourier's law, we get

$$q_x = -kA_c \frac{dT}{dx} \tag{2}$$

$$q_{x+dx} = q_x + \frac{dq_x}{dx} dx \tag{3}$$

Substituting Equation 2 into Equation 3, we obtain Equation 4 as follow.

$$q_{x+dx} = -kA_c\frac{dT}{dx} - k\frac{d}{dx}\left(A_c\frac{dT}{dx}\right)dx \tag{4}$$

The convection heat transfer rate is expressed as follow.

$$dq_{conv} = hdA_s(T - T_\infty) \tag{5}$$

A_c is cross-sectional area and dA_s is surface area of the differential element. By substituting Equations 2, 4, and 5 into Equation 1, we get the following equation.

$$\frac{d}{dx}\left(A_c\frac{dT}{dx}\right) - \frac{h}{k}\frac{dA_s}{dx}(T - T_\infty) = 0 \tag{6}$$

The Equation 6 can be written as

$$\frac{d^2T}{dx^2} + \left(\frac{1}{A_c}\frac{dA_c}{dx}\right)\frac{dT}{dx} - \left(\frac{1}{A_c}\frac{h}{k}\frac{dA_s}{dx}\right)(T - T_\infty) = 0 \tag{7}$$

Hollow Hybrid Fin

Hollow hybrid fin (HHF) has a uniform cross-sectional area, thus A_c is constant. A_s is total surface area of inner surface area (A_i) and outer surface area (A_o) and equals Px where A_s is the surface area measured from the base to x and P is the fin perimeter.

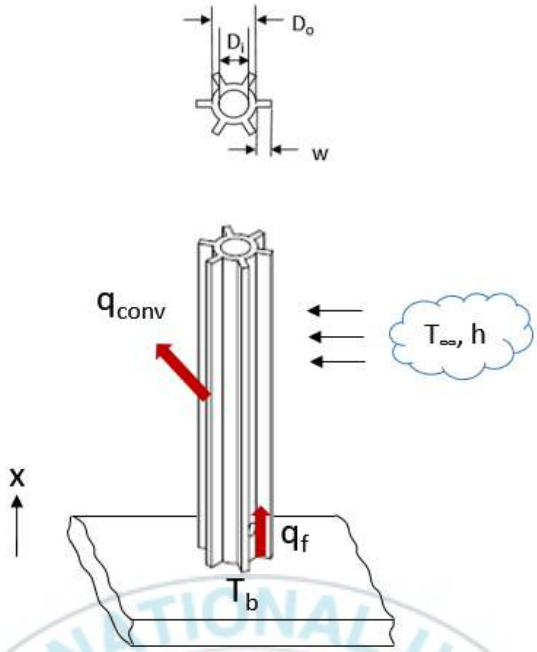

Figure 2. A hollow hybrid fin boundary condition

From Figure 2, outer and inner surface areas of the HHF are described as follow.

$$A_i = P_i x \tag{8}$$

$$A_o = P_o x + 12Wx \tag{9}$$

where W is the width of radial plate fin. The total surface area (A_s) is written as

$$A_s = (P_i + P_o + 12W)x \tag{10}$$

Then,

$$\frac{dA_c}{dx} = 0 \tag{11}$$

$$\frac{dA_s}{dx} = P = P_i + P_o + 12W \tag{12}$$

Therefore, the energy equation of the fin becomes

$$\frac{d^2T}{dx^2} - \frac{hP}{kA_c}(T - T_\infty) = 0 \tag{13}$$

An excess temperature (θ) is defined as shown in Equation 14 to simplify the above equation.

$$\theta(x) = T_{(x)} - T_\infty \tag{14}$$

Since T_∞ is constant, then $d\theta/dx = dT/dx$. Accordingly, the energy equation becomes

$$\frac{d^2\theta}{dx^2} - m^2\theta = 0 \tag{15}$$

where

$$m^2 = \frac{hP}{kA_c} \tag{16}$$

Equation 15 is linear, homogenous, and second order differential equation with constant coefficients. The general solution for the equation is

$$\theta(x) = C_1 e^{mx} + C_2 e^{-mx} \tag{17}$$

To obtain C_1 and C_2 values, two boundary conditions are determined. The first boundary condition is at fin base with constant temperature.

$$\theta_{(0)} = T_{(b)} - T_{\infty} = \theta_{(b)} \tag{18}$$

where T_b is base temperature and T_∞ is fluid temperature around the fin.

Fin Tip Condition: thick HHF

The second boundary condition can be evaluated at fin tip. For thick HHF, assume that there is convection heat transfer from the fin tip.

$$hA_c\left[T_{(L)} - T_{\infty}\right] = -kA_c \left.\frac{dT}{dx}\right|_{x=L} \tag{19}$$

$$h\theta_{(L)} = -k \left.\frac{d\theta}{dx}\right|_{x=L} \tag{20}$$

The rate at which energy is transferred to the fluid by convection from the tip should be equal the rate at which energy reaches the tip by conduction through the fin. Substituting equation 17 into equations 18 and 20 for x=0 and for x=L, then we obtain

$$\theta_{(b)} = C_1 + C_2 \tag{21}$$

and

$$(C_1 e^{mL} + C_2 e^{-mL})h = (C_2 e^{-mL} - C_1 e^{mL})km \tag{22}$$

using some manipulation, C_1 and C_2 are defined as follow

$$C_1 = \frac{\theta_b e^{-mL}(km - h)}{e^{mL}(h + km) + e^{-mL}(km - h)} \tag{23}$$

$$C_2 = \theta_b - \frac{\theta_b e^{-m}\ (km - h)}{e^{mL}(h + km) + e^{-mL}(km - h)} \tag{24}$$

Substitute Equation 23 and 24 into the equation 17, so we obtain Equation 25.

$$\theta(x) = \left(\frac{\theta_b e^{-mL}(km - h)}{e^{mL}(h + km) + e^{-mL}(km - h)}\right) e^{mx} + \left(\theta_b - \frac{\theta_b e^{-mL}(km - h)}{e^{mL}(h + km) + e^{-mL}(km - h)}\right) e^{-mx} \tag{25}$$

After some manipulation, we get the following equation.

$$\frac{\theta(x)}{\theta_b} = \frac{\dfrac{e^{-m(L-x)} + e^{m(L-x)}}{2} + \dfrac{e^{m(L-x)}\left(\dfrac{h}{km}\right) - e^{-m(L-x)}\left(\dfrac{h}{km}\right)}{2}}{\dfrac{e^{mL} + e^{-mL}}{2} + \dfrac{e^{mL}\left(\dfrac{h}{km}\right) - e^{-mL}\left(\dfrac{h}{km}\right)}{2}} \tag{26}$$

Applying further manipulation, the equation becomes

$$\frac{\theta(x)}{\theta_b} = \frac{\cosh m(L - x) + \dfrac{h}{mk}\sinh m(L - x)}{\cosh mL + \dfrac{h}{mk}\sinh mL} \tag{27}$$

Conservation energy dictates that the rate heat transferred by convection from the fin must equal the rate at which it is conducted through the base of the fin. The total heat transferred from the entire fin is

$$q_f = \int_{A_f} h[T(x) - T_\infty]dA_s \tag{28}$$

$$q_f = \int_{A_f} h\theta(x)dA_s \tag{29}$$

Applying the temperature distribution, then

$$q_f = \int_0^L hP\theta_b \left(\frac{\cosh m(L-x) + \frac{h}{mk}\sinh m(L-x)}{\cosh mL + \frac{h}{mk}\sinh mL} \right) \tag{30}$$

Therefore, the heat dissipated from the fin is as follow.

$$q_f = \sqrt{hPkA_c}\theta_b \frac{\sinh mL + \frac{h}{mk}\cosh mL}{\cosh mL + \frac{h}{mk}\sinh mL} \tag{31}$$

Fin Tip Condition: thin HHF

For thin HHF, we can assume that the heat transfer from fin tip is negligible. Therefore, the fin tip can be treated as adiabatic.

$$\left.\frac{d\theta}{dx}\right|_{x=L} = 0 \tag{32}$$

Substitute equation 17 into equations 18 and 32 for x=0 and for x=L, then

$$\theta_{(b)} = C_1 + C_2 \tag{33}$$

and

$$C_1 e^{mL} - C_2 e^{-mL} = 0 \tag{34}$$

After some manipulation, C1 and C2 are obtained as follow.

$$C_1 = \frac{\theta_b^{-emL}}{(e^{mL} + e^{-mL})} \tag{35}$$

$$C_2 = \theta_b - \frac{\theta_b^{-emL}}{(e^{mL} + e^{-mL})} \tag{36}$$

Substitute the equations 35 and 36 into the equation 17, then we get Equation 37.

$$\theta(x) = \frac{\theta_b^{-emL}}{(e^{mL} + e^{-mL})} e^{mx} + \left(\theta_b - \frac{\theta_b^{-emL}}{(e^{mL} + e^{-mL})}\right) e^{-mx} \tag{37}$$

The temperature distribution is

$$\frac{\theta(x)}{\theta_b} = \frac{\cosh m(L-x)}{\cosh mL} \tag{38}$$

Substitute equation 38 into the equation 29, the heat transfer from the fin is

$$q_f = \int_0^L hP\theta_b \left(\frac{\cosh m(L-x)}{\cosh mL}\right) \tag{39}$$

Thus, we obtain the heat dissipation from the fin as follow.

$$q_f = \sqrt{hPkA_c}\theta_b \tanh mL \tag{40}$$

2.2 Natural Convection

Convection is heat transport by a moving fluid due to the temperature difference. The fluid carries away energy from the heat source. This heat transfer mode is defined by Newton's law of cooling as follow.

$$q'' = h(T_s - T_\infty) \tag{41}$$

where h is the convective heat transfer coefficient, T_s is temperature of the surface, T_∞ is temperature of fluid, and q'' is the heat flux of convection. The temperature difference is proportional to the heat flux. The coefficient of convection heat transfer is an important constant for calculating the heat flux. This coefficient is influenced by the surrounding such as structure of the body, properties and velocity of the fluid, and the fluid motion.

The fluid motion that induced by buoyancy forces without the present of forced velocity is called natural convection. In this case, the body force is gravity. Buoyancy forces occur when density gradient exist associated with the difference of the fluid temperature. As widely known, generally the fluid density decreases when the temperature increases. The hot fluid will move upwards while the cold fluid goes down. This is causing fluid flow around the hot surface.

An illustration is shown in Figure 3 to demonstrate heat transfer by natural convection. Assume a vertical plate is immersed in a quiescent fluid. The plate surface (T_s) has a higher temperature than the fluid (T_∞). Therefore, the fluid temperature rises and that condition generates heat transfer induced by buoyancy forces. Fluid velocity at the surface and at the boundary are zero due to viscous forces. Correspondingly, the fluid around the surface affected by the surface temperature develop temperature gradient along the y-axis until the temperature reaches the fluid temperature.

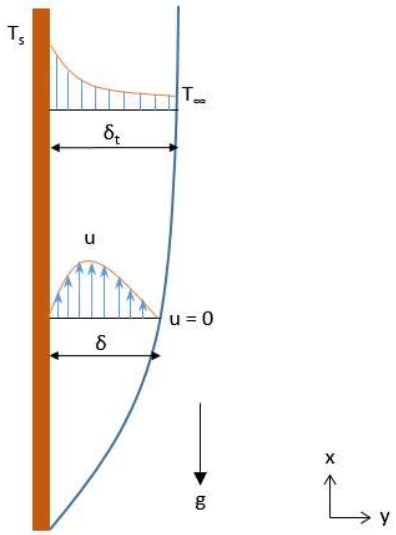

Figure 3. Temperature and velocity profiles of natural convection heat transfer

2.3 Dimensionless Parameters

The behavior of natural convection depends on boundary conditions and geometry. Several dimensionless parameters play a significant contribution in describing natural convection phenomena such as the characteristic of the fluid and the turbulence of the flow. The dimensionless parameters are described in this section.

Grashof Number

The Grashof number defines fluid flow driven by natural convection. Since the natural convection is mainly due to buoyancy and viscous forces, this non-

dimensional number estimates nature of the fluid using the ratio of the above-mentioned forces. Equation 42 defines the Grashof number.

$$\mathrm{Gr} = \frac{g\beta(T_s - T_\infty)L_c^3}{v^2} \tag{42}$$

where β is the thermal expansion coefficient, g is the acceleration of gravity, T_s is temperature of the surface, T_∞ is the free stream temperature, ν is kinematic viscosity, and L_c is the characteristic length of the structure.

This number determines flow type of the fluid whether it is laminar or turbulent. The transition value of Grashof number of natural convection ranges from 10^8 to 10^9. The fluid is laminar if the value less than 10^8 and it becomes turbulent for the value more than 10^9.

Prandtl Number

The fluid property that defined by the ratio of kinematic viscosity and thermal diffusivity is called Prandtl number. This number is helpful for investigating natural convection behavior where heat transfer and fluid movement are primary aspect of the condition. The Prandtl number is expressed as follow.

$$\mathrm{Pr} = \frac{c_p \mu}{k} = \frac{v}{\alpha} \tag{43}$$

where ν is the kinematic viscosity of the fluid, α is the thermal diffusivity of the

fluid, c_p is the heat capacity of the fluid, μ is the dynamic viscosity of the fluid, and k is thermal conductivity of the fluid.

The Prandtl number shows the heat transfer process occurred in the fluid by both conduction and convection. Therefore, this number represents the boundary layers of velocity and thermal of the fluid. When the Prandtl number is unity, both velocity and thermal boundary layers will have the same thickness. The value lower than one (1) indicates the heat diffuses quicker compared to the fluid velocity, which means the thermal boundary layer is greater than velocity boundary layer, and vice versa.

Rayleigh Number

In natural convection, the combination of the two important dimensionless parameters above produces a dimensionless parameter that determines the flow turbulence. This dimensionless parameter is called Rayleigh number. The following equation defines the Rayleigh number.

$$\mathrm{Ra} = \mathrm{Gr}\ .\mathrm{Pr} = \frac{g\beta(T_s - T_\infty)L_c^3\ Pr}{v^2} \tag{44}$$

This Rayleigh number indicates the flow regime whether it is laminar or turbulent. The fluid flow starts to become turbulent when the Rayleigh number reach 10^9. Figure 4 shows the boundary conditions based on the Rayleigh number value.

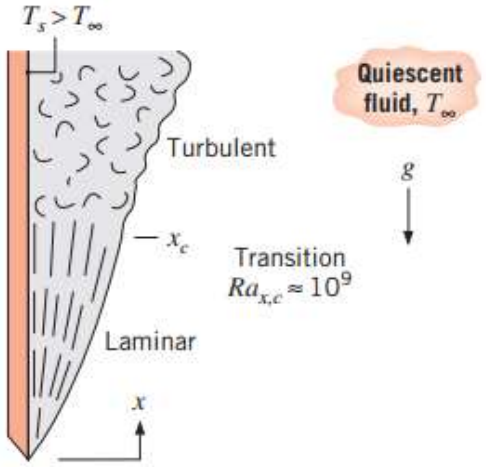

Figure 4. Boundary layer of natural convection around the vertical plate

Nusselt Number

Nusselt number is a dimensionless parameter that defines a ratio between convective and conductive heat transfer that occurs in a fluid. The following equation formulates the Nusselt number.

$$\mathrm{Nu} = \frac{q''_{conv}}{q''_{cond}} = \frac{h_c \Delta T}{k \Delta T / L_c} = \frac{h_c L_c}{k} \tag{45}$$

where: q''_{conv} is the convection heat flux, q''_{cond} is the conduction heat flux, h_c is the coefficient of convection heat transfer, ΔT is the temperature difference between the hot and cold of fluid, k is the coefficient of conduction heat transfer, and L_c is length characteristic of the geometry.

This number is employed to calculate the heat transfer coefficient in natural convection case. The Nusselt number is related with the Rayleigh number as expressed below.

$$\mathrm{Nu} = \mathrm{f}(\mathrm{Gr}, \mathrm{Pr}) \tag{46}$$

PUKYONG NATIONAL UNIVERSITY
부경대학교

III. Numerical Modelling

The aim of the numerical modelling is to understand the thermal behavior and obtain the predictive data of the HHFs and fin arrays. The first and second sections describe structure of the hollow hybrid fin and fin array, respectively. The next section is an explanation of numeric modelling which includes governing equations, assumptions, solution methods, and mesh independency. The fourth and fifth sections are about the numerical models of the HHF and the fin array with their configurations.

3.1 Hollow Hybrid Fin

A hollow hybrid fin (HHF) is a hollow pin fin integrated with radially-placed plate fins and having a perforation near the fin base. Figure 5 depicts the structure of a HHF that consist of outer diameter (D_o), inner diameter (D_i), perforation diameter (D_p), width of plate fin (W), and height of fin (H). The presence of an inner diameter provides an advantage in reducing fin weight and allows internal airflow through the perforation due to the chimney effect. Therefore, internal flow and external flow exist on this HHF. The plate fins enhance surface area of the fin, which improve the fin performance.

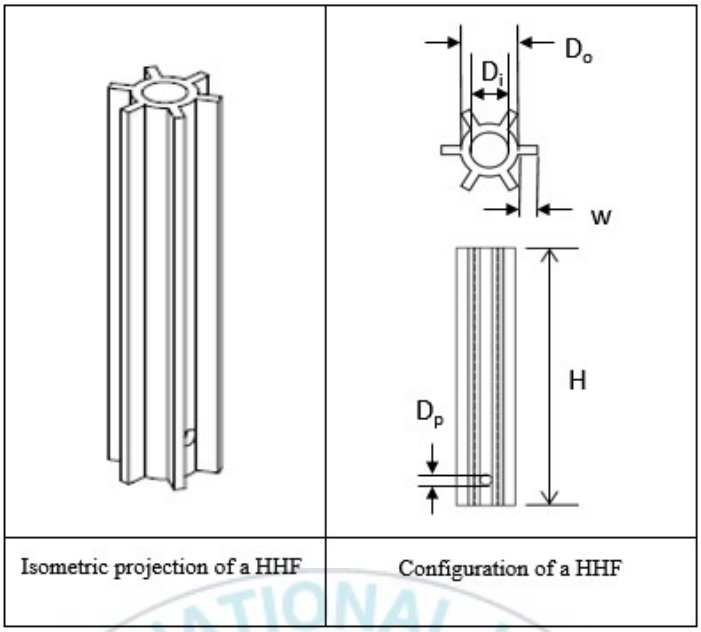

Figure 5. A HHF structure

3.2 Hollow Hybrid Fin Array

Hollow hybrid fin array is a staggered arrangement of HHFs with a certain fin spacing (S). Number of fins is associated with the fin spacing. HHF array configurations utilize broad range variation of outer diameter (D_o), inner diameter (D_i), fin height (H), and fin spacing (S) with the same base dimension, which is 75 mm x 75 mm of length and width with 5 mm of thickness. Figure 6 shows the HHF array structure.

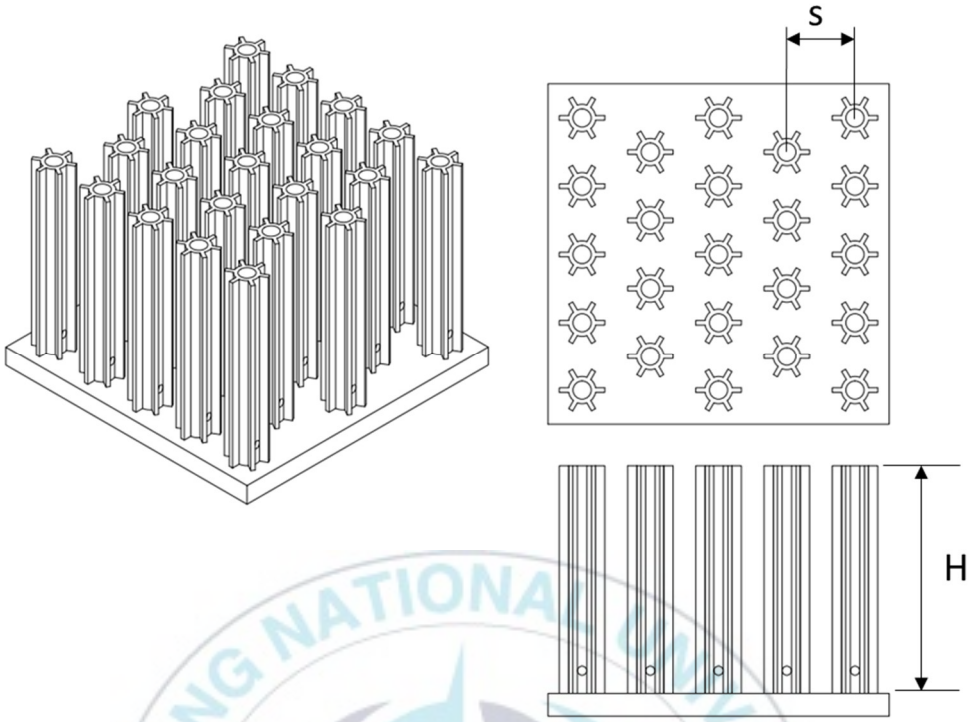

Figure 6. A HHF array structure

3.3 Numerical Modelling

The computational fluid dynamics (CFD) models of the HHFs and the HHF arrays were carefully generated to obtain wide-ranging thermal data and then evaluated the numerical results to understand their thermal behavior. ANSYS ICEM-CFD was used for meshing and Fluent was employed to solve the numerical calculation. The numerical results were obtained and evaluated utilizing CFD post. The radiation effect is excluded in the numerical computations as this study only focuses on analyzing natural convective heat transfer. The airflow was assumed as

incompressible fluid and steady state condition. Boussinesq approximation was applied for natural convection where the density variations only affect the buoyancy force and are neglected them in the inertial term (mass and acceleration). The HHFs and HHF arrays materials were aluminum 6063.

Governing Equations

Computations of HHFs and HHF arrays used the following governing equations (47-52) [27, 28].

The continuity equation is of the form

$$\frac{\partial u}{\partial x}+\frac{\partial v}{\partial y}+\frac{\partial w}{\partial z}=0 \tag{47}$$

The momentum equations are given by

$$u\frac{\partial u}{\partial x}+v\frac{\partial u}{\partial y}+w\frac{\partial u}{\partial z}=-\frac{1}{\rho}\frac{\partial P}{\partial x}+\nu\left(\frac{\partial^2 u}{\partial x^2}+\frac{\partial^2 u}{\partial y^2}+\frac{\partial^2 u}{\partial z^2}\right) \tag{48}$$

$$u\frac{\partial v}{\partial x}+v\frac{\partial v}{\partial y}+w\frac{\partial v}{\partial z}=-\frac{1}{\rho}\frac{\partial P}{\partial y}+\nu\left(\frac{\partial^2 v}{\partial x^2}+\frac{\partial^2 v}{\partial y^2}+\frac{\partial^2 v}{\partial z^2}\right) \tag{49}$$

$$u\frac{\partial w}{\partial x}+v\frac{\partial w}{\partial y}+w\frac{\partial w}{\partial z}=-\frac{1}{\rho}\frac{\partial P}{\partial z}+\nu\left(\frac{\partial^2 w}{\partial x^2}+\frac{\partial^2 w}{\partial y^2}+\frac{\partial^2 w}{\partial z^2}\right)+g\beta\ \ (T-T_\infty) \tag{50}$$

The energy equation of fluid region is written as

$$u\frac{\partial T}{\partial x}+v\frac{\partial T}{\partial y}+w\frac{\partial T}{\partial z}=\alpha\ \left(\frac{\partial^2 T}{\partial x^2}+\frac{\partial^2 T}{\partial y^2}+\frac{\partial^2 T}{\partial z^2}\right) \tag{51}$$

The energy equation of solid region is expressed as

$$\frac{\partial^2 T}{\partial x^2} + \frac{\partial^2 T}{\partial y^2} + \frac{\partial^2 T}{\partial z^2} = 0 \tag{52}$$

where u, v, and w are velocities in x, y, and z directions, α is thermal diffusivity, β is volumetric thermal expansion constant, ρ is density, ν is kinematic viscosity, P is pressure, g is gravity, T is temperature, and T_∞ is the free stream temperature.

Summary of Assumptions

Numerical calculation of the HHFs and fin arrays used several assumptions as described below.

1. Material of the HHFs and fin arrays is aluminum 6063;
2. The working fluid is air;
3. Incompressible flow, i.e., Mach number Ma<0.3 [33];
4. Incompressible ideal gas;
5. Laminar flow, steady state condition, i.e., Rayleigh number $Ra<10^9$ [33];
6. Three dimensional flow and heat transfer;

Solution Methods

The solution methods as shown in Table 1 were selected according to the predetermined boundary conditions for all of the CFD models of HHFs and HHF

arrays. Viscous model was laminar due to the Rayleigh number lower than $1x10^9$. Solver type was pressure based for incompressible flow. SIMPLE method applied to the pressure-velocity coupling for steady-state calculations. Pressure discretization was based on body force weighted. The second-order upwind was chosen for both energy and momentum discretization.

Table 1. Solution methods of numerical calculations

Solution methods	
Density model	Incompressible ideal gas
Viscous model	Laminar
Pressure-velocity coupling	SIMPLE
Solver type	Pressure based
Spatial discretization	
Pressure	Body force weighted
Momentum	Second-order upwind
Energy	Second-order upwind
Gradient	Least squares cell based

Mesh Independence

Before performing the numerical calculations, it is important to analyze the mesh independency to ensure the reliability of the results. The mesh independence of CFD models of HHFs and HHF arrays was carefully investigated by increasing the number of elements so that the thermal resistance discrepancies were less than 1%. Thus, the numerical solutions were converge and vigorous.

Evaluation of mesh independency of a fin array is shown in Figure 7 as a

study case. The number of mesh elements were examined to their thermal resistance. The result indicates that increasing the element number more than 2.9 million did not give a different value in the numerically-obtained thermal resistance. Therefore, the numerical study was carried out using the number of elements 2.9 million.

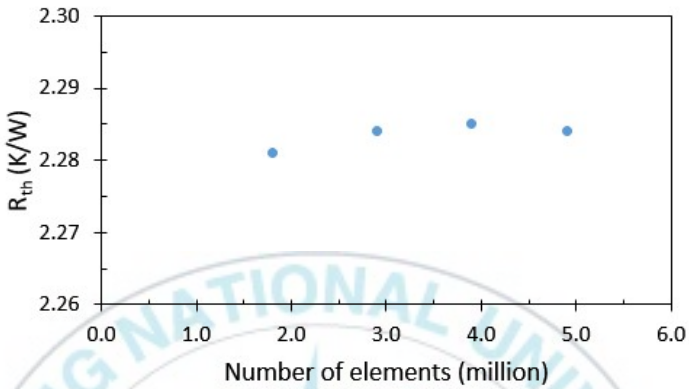

Figure 7. Evaluation of mesh independence of fin array

3.4 CFD Model of HHF

Fin height of the HHF CFD models are 5, 20, 75, and 100 mm with 14 combinations of outer diameter and inner diameter as displayed in Table 2. The total configurations are 56 variations of HHF structures. In this study, we focused on diameters and height effects. Thus, the plate fin width is fixed with the value of 2 mm. Bases of the HHFs were uniformly heated at temperature 50, 70, and 90°C. The ambient temperature was 25°C for all of numerical calculations. Total of CFD models for the HHFs is 168 models. Figure 8 shows the numerical model and boundary conditions of the HHFs. Numerical calculations used CFD models with

mesh elements of 60 – 500 thousands. Table 3 summarizes the computational settings of HHFs.

Table 2. Variations of outer diameter and inner diameter of HHF configurations.

Type	D_o (mm)	D_i (mm)	W (mm)
1	3	1	2
2	6	1	2
3	6	2	2
4	6	4	2
5	10	1	2
6	10	2	2
7	10	4	2
8	10	6	2
9	10	8	2
10	20	1	2
11	20	6	2
12	20	10	2
13	20	16	2
14	20	18	2

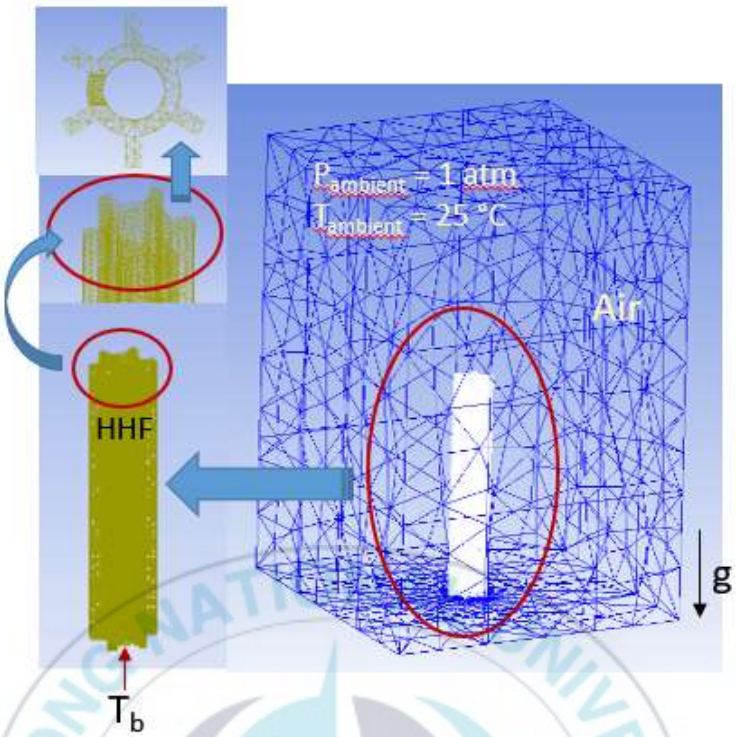

Figure 8. The numerical model and boundary conditions of a HHF

Table 3. Summary of computational settings of HHFs

Computational settings	
Material of HHF	Aluminum 6063
Fluid	Incompressible and steady flow
Number of elements	60k – 500k elements
Element type	Tetra
Air Pressure	1 atm
Air temperature	25° C
Fin base temperature	50, 70, 90°C

3.5 CFD Model of HHF Array

CFD models of the HHF arrays contained 12 configurations with three variations of fin height (20, 75, and 200 mm). Outside diameter of the HHF arrays are 4 and 20 mm, while inside diameters are 1, 3 and 19 mm. Width of the pin fin is 2 mm and the fin spacing are 10, 15, 25, and 40 mm. The detail of fin arrays configurations are shown in Table 4. Figure 9 illustrates the numerical model and boundary conditions of the HHF array. The HHF arrays bases were uniformly heated at temperatures 50, 70, 90, and 120°C. The numerical study of HHF arrays was calculated with 25°C of ambient temperature. Total of 48 3D-models of HHF arrays were evaluated. CFD models with total mesh elements of 2-25 millions were utilized to generate numerical results. The computational settings of HHF arrays are summarized in Table 5.

Table 4. Summary of fin arrays configurations

Type	N	S (mm)	H (mm)	W (mm)	D_o (mm)	D_i (mm)	D_p (mm)
1	23	15	20	2	4	3	1.5
2	8	25	20	2	4	1	1.5
3	46	10	20	2	4	1	1.5
4	5	40	20	2	20	1	6
5	23	15	75	2	4	3	1.5
6	8	25	75	2	4	1	1.5
7	5	40	75	2	20	19	6
8	5	40	75	2	20	1	6
9	23	15	200	2	4	3	1.5
10	8	25	200	2	4	1	1.5
11	46	10	200	2	4	3	1.5
12	5	40	200	2	20	1	6

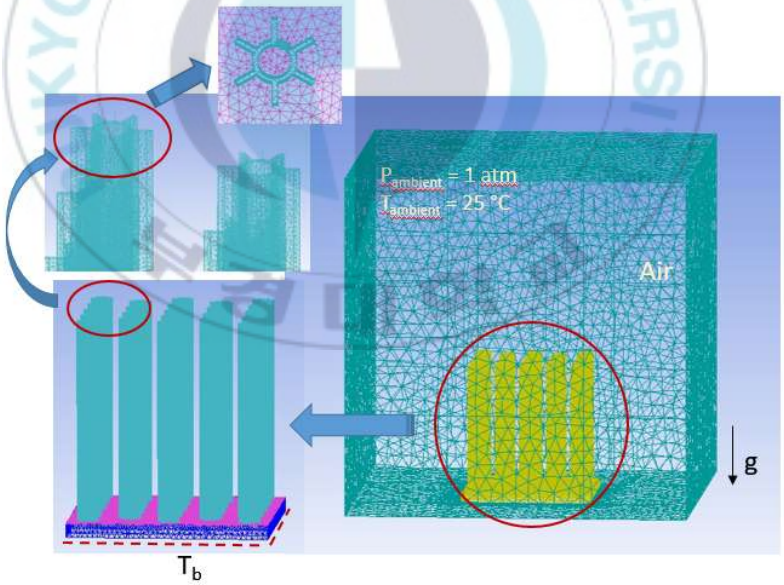

Figure 9. The numerical model and boundary conditions of a HHF array

Table 5. Summary of computational settings and solution methods of HHF arrays

Computational settings	
Material of HHF arrays	Aluminum 6063
Fluid	Incompressible and steady flow
Number of elements	2 – 25M elements
Element type	Tetra
Air Pressure	1 atm
Air temperature	25° C
Base temperature of HHF arrays	50, 70, 90, 120°C

PUKYONG NATIONAL UNIVERSITY
부경대학교

IV. Experimental Validation

The purpose of this chapter is to validate the numerical models through the experimental study. This chapter is divided into three sections. First, test rig of experiment are described including the required equipment and components. Second, sample preparations of the HHF and the fin array are explained. The last section describes the measurement procedure for validation process.

4.1 Test Rig Setup

The test rig for the HHFs and fin arrays experiment was assembled and placed in a closed laboratory. The equipment and components used for the experiments are shown in Table 6. A DC power supply was utilized to provide electric current to the heaters. T-type thermocouples sensed the temperatures of the HHFs and HHF arrays. Data logger was utilized to record data from the thermocouples. The measured temperatures were displayed on the DAQ PC. IR thermography was applied to verify the temperature measurement of the thermocouples. A sample stand made from polyethylene terephthalate (PET) utilized to hold the samples.

Table 6. Equipment and components of experimental setup

Equipment of HHF and HHF array experiments	
DC power supply	Agilent 6655A
T-type thermocouple	Omega Thermocouple
Data logger	Agilent 34970A
Data acquisition PC	DAQ PC
IR Camera	FLIR T440
Sample stand	Polyethylene Terephthalate (PET)
Components of HHF experiment	
Ceramic heater	10 x 10 mm
Insulation layers	
Glass wool	40 x 40 x 10 mm
Polytetrafluoroethylene (PTFE)	40 x 40 x 10 mm
Polyethylene Terephthalate (PET)	100 x 100 x 100 mm
Components of HHF array experiment	
Polyimide heater	75 x 75 mm
Insulation layers	
Glass wool	100 x 100 x 10 mm
Polytetrafluoroethylene (PTFE)	100 x 100 x 10 mm
Polyethylene Terephthalate (PET)	100 x 100 x 100 mm

Then, the equipment and measurement devices used for the experiment were arranged as depicted in Figure 10.

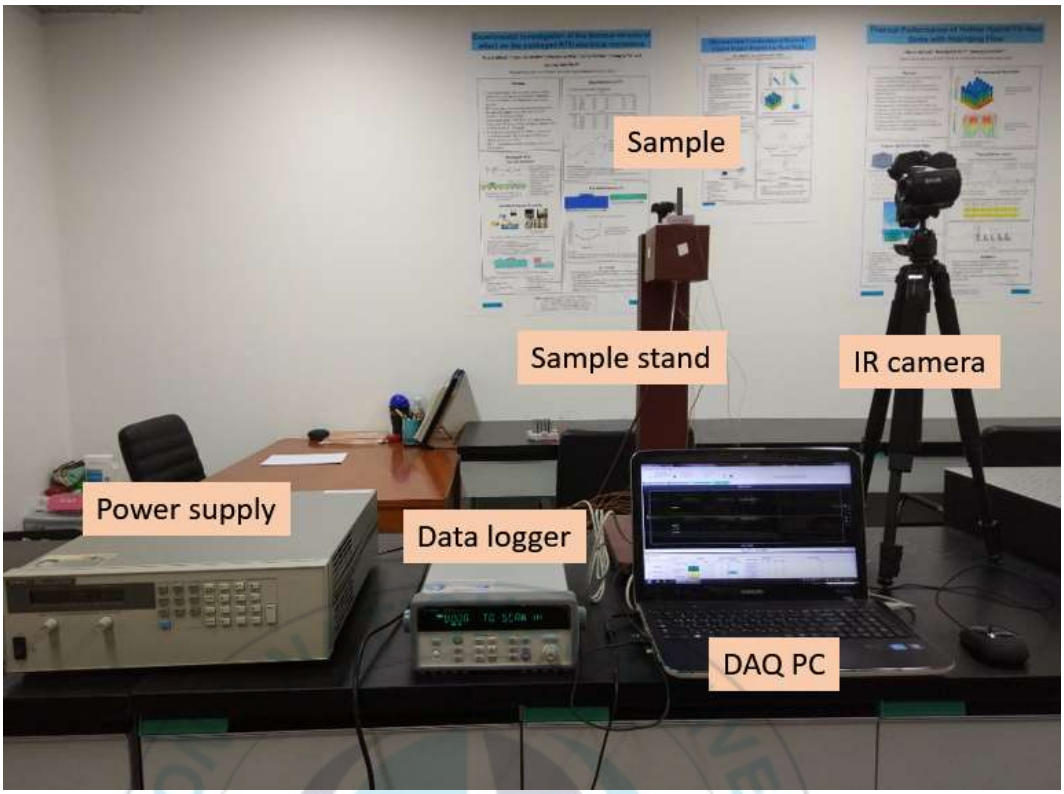

Figure 10. Experimental setup for the HHF and the fin array

Figure 11 and Figure 12 display the schematic of the test rig setup for the HHF and the fin array, respectively. As can be seen from the figures, the only difference in the setup was the sample settings. For further details, the sample preparation is discussed in the next section.

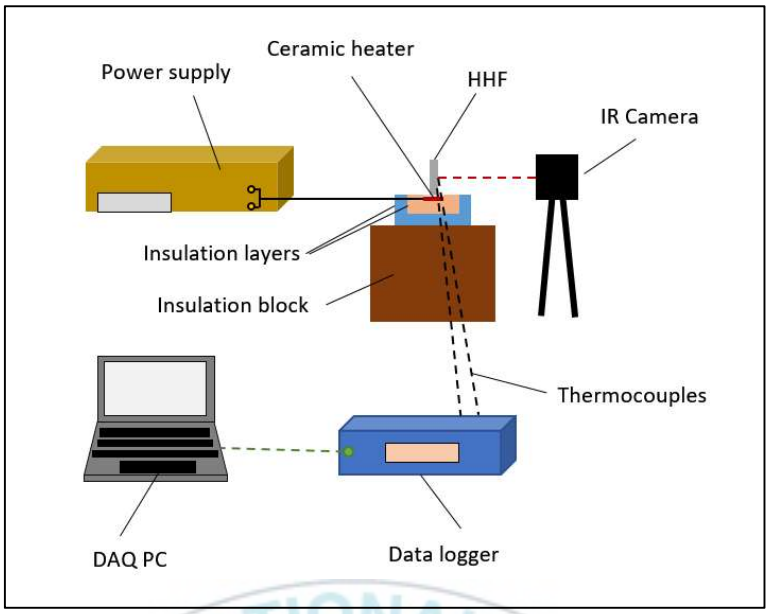

Figure 11. The schematic of the HHF test rig

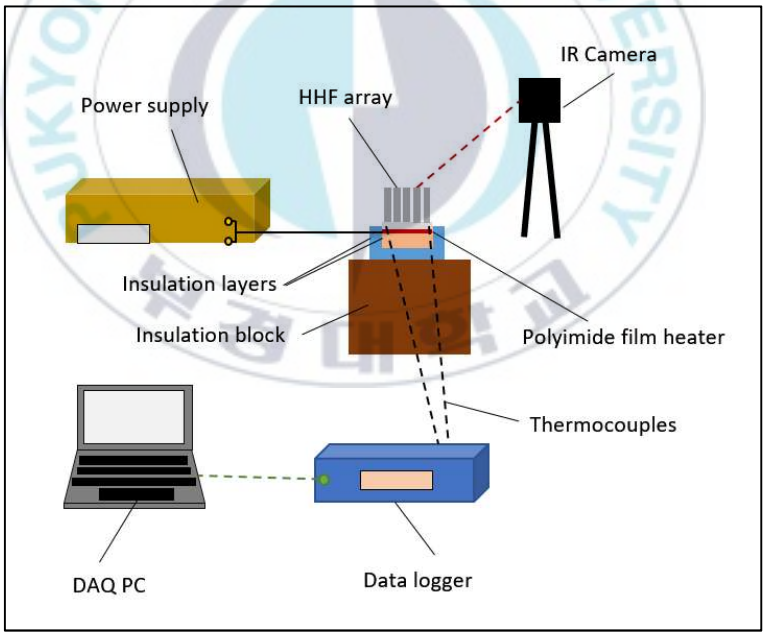

Figure 12. The schematic of the HHF array test rig

4.2 Sample Preparation

The HHFs were carefully fabricated with the dimensions as detailed in Table 7. The material used for the samples was aluminum 6063 in consideration of its properties such as easy manufacturability and high thermal conductivity. The representative dimensions were chosen due to the manufacturing limitations. For the fin array sample, total of 23 fins were tightly assembled into the baseplate to minimize the contact resistance. The surface of the HHF and HHF array were black painted, thus radiation effects from surrounding is minimized.

Table 7. Dimensions of samples for experiment

Parameter	Dimension (mm)
Fin height	50
Outer diameter	6
Inner diameter	4
Perforation diameter	1
Fin width	2
Fin spacing (for fin array)	15

A ceramic heater with 10 mm long and 10 mm wide was utilized to uniformly heat the base of the HHFs. The inevitable heat loss was minimized by applying the insulation layers to the samples. The composition of the insulators was a polytetrafluoroethylene (PTFE) plate with dimensions of 40 x 40 x10 mm, a glass wool layer with a thickness of 10 mm, and a polyethylene terephthalate (PET) block with dimensions of 100 x 100 x 100 mm. Two T-type thermocouples were attached

on the HHF at the middle and bottom heights. The other two T-type thermocouples were attached on the base. The HHF sample is shown in Figure 13.

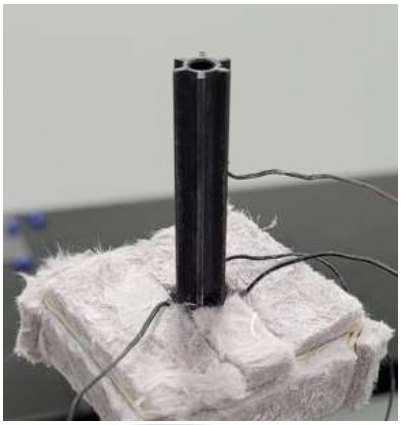

Figure 13. A hollow hybrid fin sample for experiment

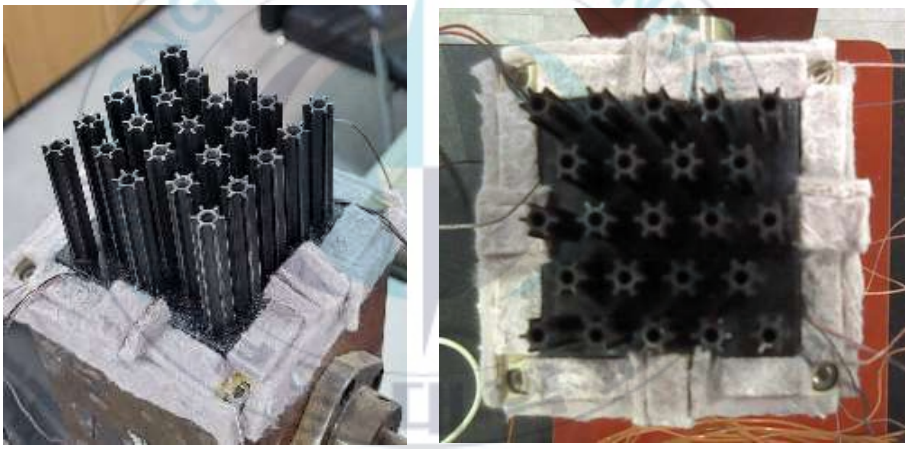

(a) (b)

Figure 14. (a) Perspective view and (b) top view of a hollow hybrid fin array sample for experiment

The HHF array experiment utilized a polyimide film heater with dimensions of 75 x 75 mm to heat the base. In this experiment, the insulation layers

consist of a polytetrafluoroethylene (PTFE) plate with dimensions of 100×100×10 mm, a glass wool layer with thickness of 10 mm, and a polyethylene terephthalate (PET) block with dimensions of 100 × 100 × 100 mm. Three T-type thermocouples were attached on the baseplate. Figure 14 depict the sample of the fin array.

4.3 Measurement Procedure

The experimental investigations were carried out to validate the CFD models of HHFs and HHF arrays by comparing the measurement of thermal resistance (R_{th}) with the numerical calculation.

$$R_{th} = \frac{T_b - T_a}{q} \tag{53}$$

where q is the heat rate, T_b is the base temperature of HHF or HHF array, and T_a is the ambient temperature.

The laboratory is a closed room and no forced airflow during the experiment. The experiment was conducted at room temperature. A sample stand was used to hold the samples by connecting it to the insulation part of the samples, namely polyethylene terephthalate (PET). The base of the HHFs and the fin arrays was uniformly heated by the heaters. The current and voltage of the power supply were set to provide the heat rate at certain value to the heaters. The T-type thermocouples attached to the samples sensed the temperatures. The thermocouples

were connected to data logger that read the measured temperatures. The measurement results were collected from DAQ PC after the steady state condition was reached. The experimentally-measured thermal resistance of the HHFs and the fin arrays was obtained using the equation 53.

PUKYONG NATIONAL UNIVERSITY
부경대학교

V. Results and Discussions

This chapter presents the numerical and experimental results of the HHFs and fin arrays. The numerical results provide the thermal and velocity fields. The measurement results of experiment with various heat dissipation are compared to the numerical data for the HHFs and arrays as a validation of the CFD models. Finally, the development of predicted Nusselt number correlations of the HHFs and arrays are described in detail.

5.1 Simulation Results

Thermal and Velocity Fields

Temperature distributions and velocity fields of the representative HHFs and HHF arrays obtained by numerical calculations are shown from Figure 15 to 18. All of the thermal and velocity fields displayed are observed at base temperature 90°C. From Figure 15, one can see that the temperature distribution of HHFs is reasonable with a decrease in temperature as it gets further from the base. The velocity fields in Figure 16 reveal external and internal air flows with well-developed symmetric flow. Similarly, Figure 17 shows that the HHF array temperature is cooler at fin tip. The temperature decreases from center of the heat sink to the edge. Both temperature and velocity fields in Figure 17 and 18 show symmetrical results that induced by natural convection. Overall, these numerical

solutions seem reasonable to denote the reliability of CFD models.

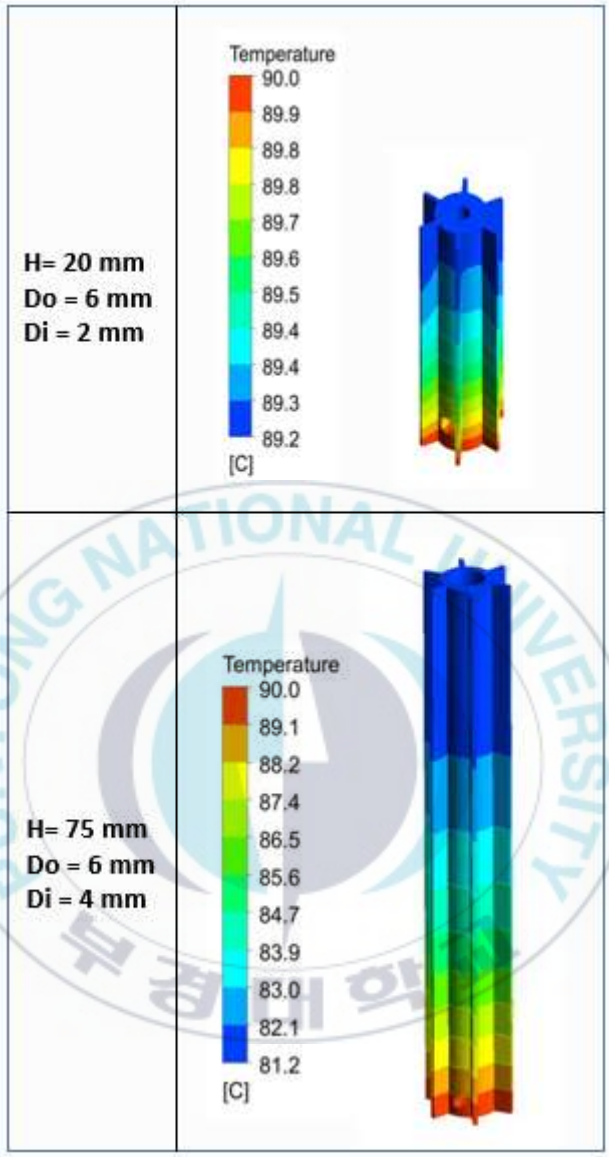

Figure 15. Temperature distribution of the HHFs

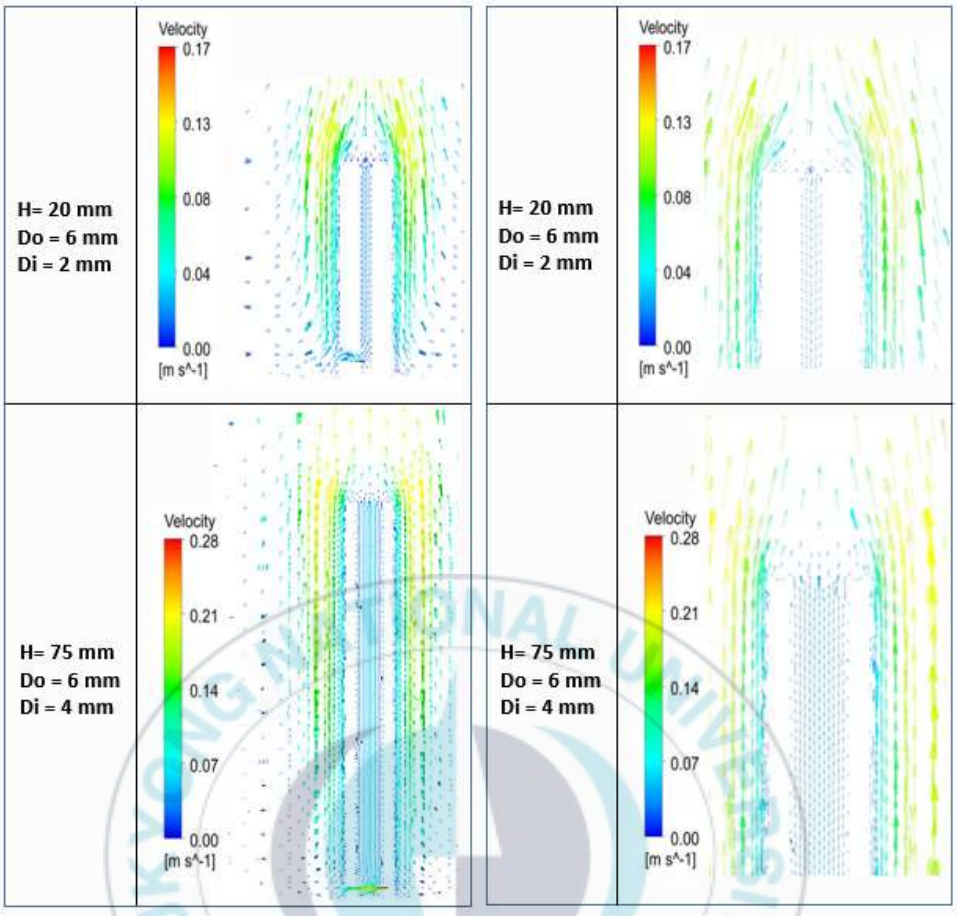

Figure 16. Velocity fields of the HHFs

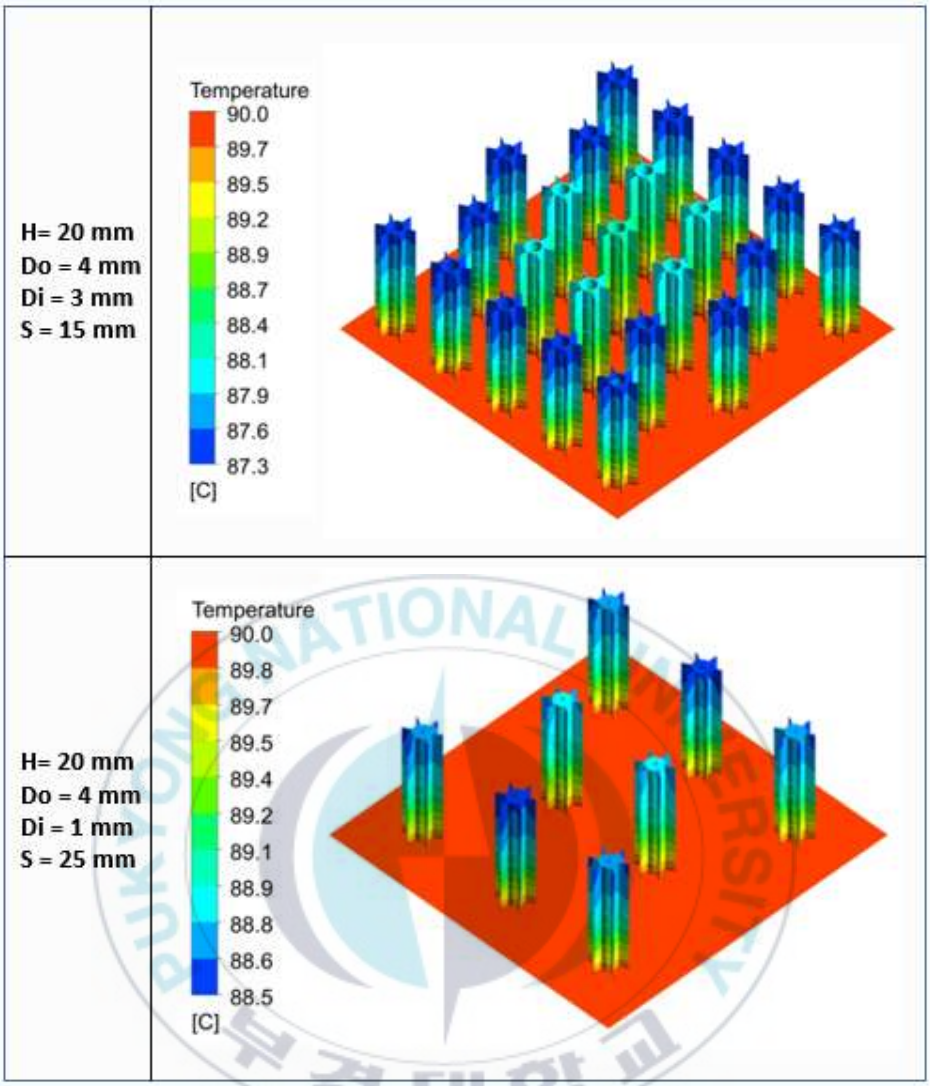

Figure 17. Temperature distribution of the HHF arrays

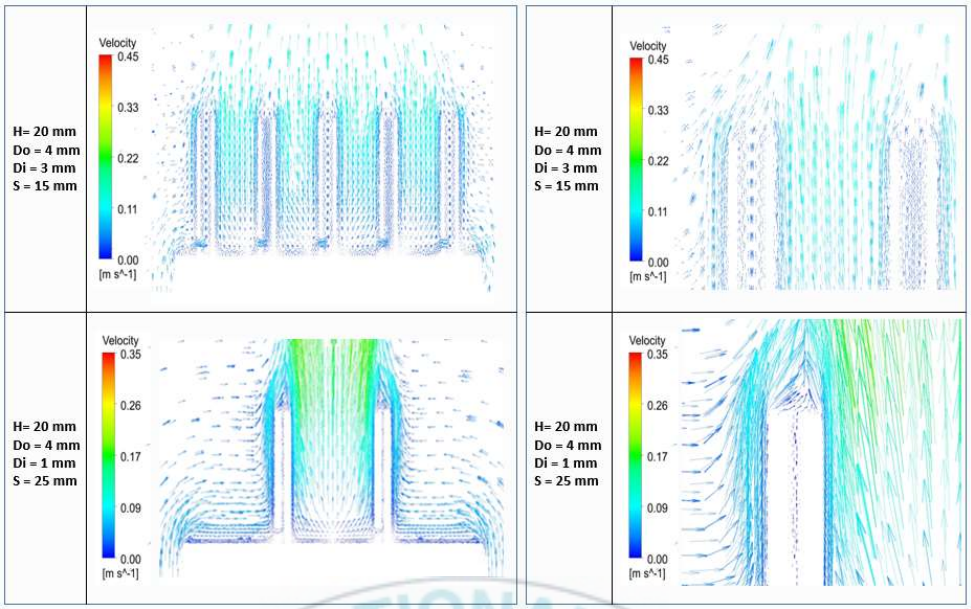

Figure 18. Velocity fields of the HHF arrays

5.2 Experimental Results

Uncertainty Calculation

During the measurement process, error propagation may happen from several factors. In this experiment, the error is mainly caused by temperature measurement and power input [29]. The T-type thermocouples are estimated to have an uncertainty of ± 0.5 °C. The measurement error of IR thermography is about ± 1 °C. The DC power supply used in this experiment has an uncertainty of 0.2 %. Uncertainty analysis was conducted by using error propagation method in physical measurements [30, 31].

Table 8. Uncertainty of the HHF and the HHFHS experiments

Type	Heat Dissipation (W)	T_b (°C)	Deviation (±°C)	Bias error (±°C)	Total uncertainty (±°C)	Uncertainty (%)
HHF	0.94	66.48	0.46	1.13	1.60	2.40
	1.46	87.55	0.22	1.18	1.39	1.59
	1.86	103.09	0.80	1.21	2.01	1.95
	2.30	120.43	0.17	1.24	1.41	1.17
	2.69	137.37	0.40	1.27	1.67	1.22
HHF array	10.0	53.69	0.50	0.61	1.11	2.07
	14.4	64.24	0.22	0.63	0.85	1.32
	20.7	76.90	0.19	0.65	0.85	1.10
	25.5	85.86	0.20	0.67	0.87	1.01
	30.0	93.45	0.33	0.69	1.02	1.09

Table 8 summarizes the uncertainty analysis of HHFs and HHF arrays experiments on several heat dissipations. The maximum uncertainties in the validation process of HHFs and HHFHSs were at the lowest heat dissipations, namely 0.94 W and 10.0 W with uncertainties of 2.40 % and 2.07 %, respectively.

Temperature Measurement

The temperature measurement utilizing T-type thermocouple validated by IR thermography. In this regard, the temperature measurement on the HHFs is used as a sample case. Figure 19 illustrates the thermography measurement on the HHF. Two T-type thermocouples were attached on the HHF at the middle and bottom heights. The measured temperatures are compared between IR camera and the T-type thermocouple.

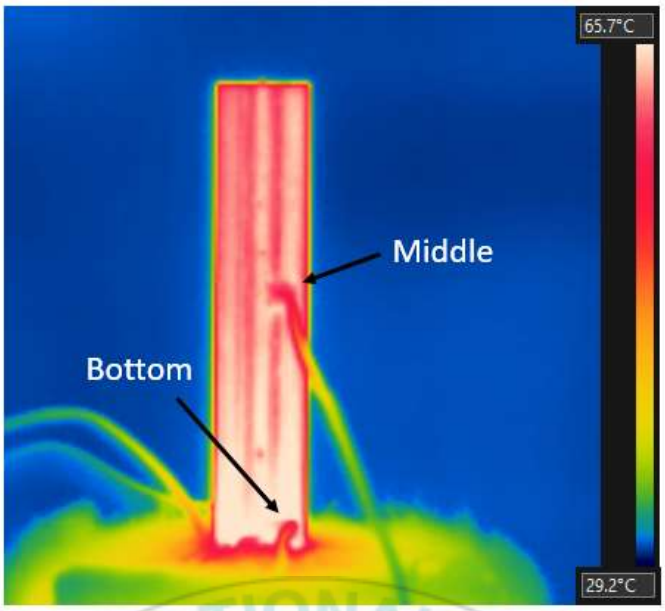

Figure 19. IR thermography of a HHF

Table 9. Temperature measurement of the HHFs

Heat Dissipation (W)	IR Camera (°C)		Thermocouple (°C)	
	Middle	Bottom	Middle	Bottom
0.94	59.0	61.9	60.5	63.6
1.46	75.6	81.1	77.2	82.1
1.86	86.1	93.2	87.7	95.0
2.30	98.6	108.0	101.3	110.3
2.69	111.7	122.6	113.8	125.0

The discrepancies of thermal measurements between the T-type thermocouple and IR thermography were lower than 3%. Thus, the T-type thermocouple measurement was reliable for the experiment.

Measurement of Thermal Resistance

The thermal resistance of the HHFs was evaluated at various heat dissipations, which are 0.94, 1.46, 1.86, 2.30, and 2.69 W. Figure 20 compares the numerically-obtained and experimentally-evaluated of thermal resistance of the HHFs. The thermal resistance between the measurement and the simulation was found to have reasonable agreement, within 10% discrepancy.

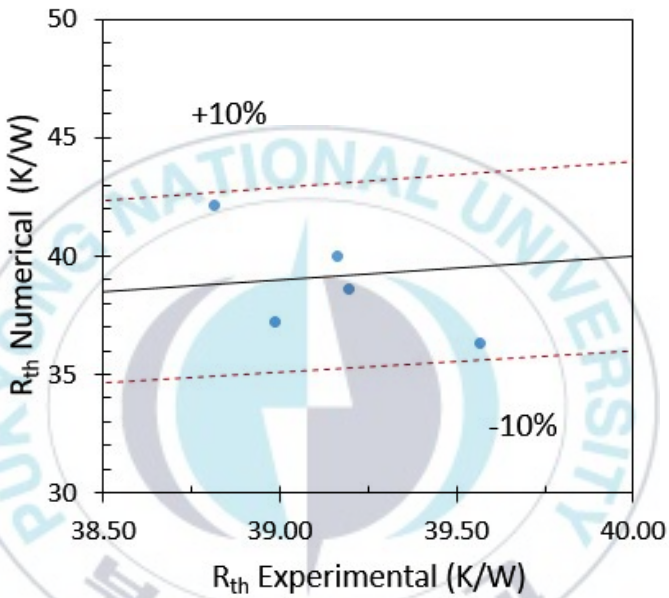

Figure 20. Numerical thermal resistance of HHFs as a function of measured thermal resistance

Figure 21 shows the comparison between numerically-obtained and experimentally-evaluated of thermal resistance of HHF arrays with heat dissipations

10.0, 14.5, 20.8, 25.5 and 30.0 W. The thermal resistance of numerical results shows a good agreement with the measurement data. The average thermal resistance discrepancy was 7%.

The inevitable heat loss still occurred despite of the installation of insulation layers and became the main reason for the difference in thermal resistance. However, the overall of the experimental results of HHFs and HHF arrays demonstrated the vigorous of CFD models for predicting the thermal behavior.

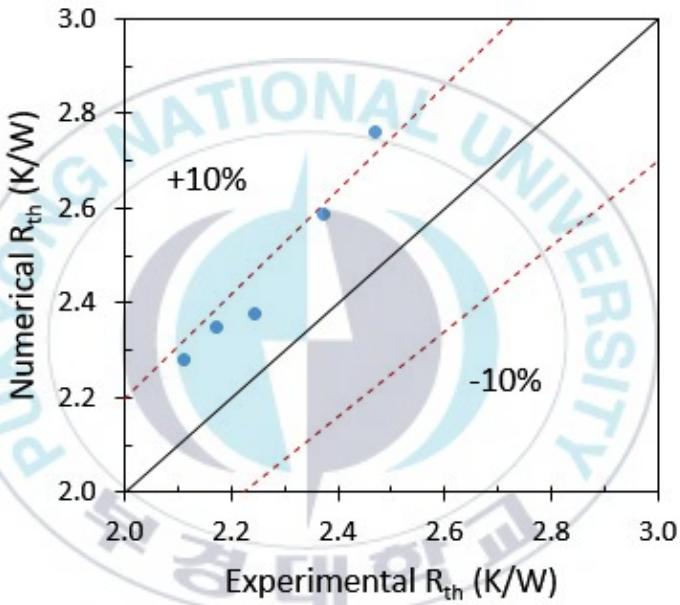

Figure 21. Numerical thermal resistance of HHF arrays as a function of measured thermal resistance

5.3 Nusselt Number Correlations

Two dimensionless parameters i.e. Nusselt number (Nu) and Rayleigh number (Ra), were employed to predict the thermal behavior of HHFs and HHF arrays with natural convection cooling. The development of Nusselt number correlations utilizes the equations 4 and 5 in Chapter II.

The fluid properties used for calculating the Rayleigh number depend on the temperature, so the film temperature was applied to quantify the fluid properties. Equation 54 defines the film temperature.

$$T_{film} = \frac{T_s + T_a}{2} \tag{54}$$

where T_s is temperature of the surface and T_a is the ambient temperature.

Nusselt number correlations for the HHFs and the HHF arrays were generated utilizing the thermal data, obtained by the CFD models, by considering Rayleigh numbers and the primary geometric parameters.

5.3.1 Nusselt Number of The HHF

The fin height was used as a characteristic length for Nusselt number and Rayleigh number of the HHFs. The predicted Nusselt number of HHFs were expressed as follow.

$$Nu_F^{cor} = C_1 . Ra^{C_2} \left(\frac{D_o - D_i}{W}\right)^{C_3} \left(\frac{H}{D_o}\right)^{C_4} \left(\frac{D_i}{W}\right)^{C_5} \tag{55}$$

where D_o is outer diameter, D_i is inner diameter, W is width of pin fin, and H is height of the fin.

The HHF correlations were defined for two regions of Reynolds number, which are low range Ra (Ra <40,000) and high range Ra (Ra 40,000-4,000,000). Table 10 details the values of empirical constants of the HHFs correlations.

Table 10. Empirical constants of Nusselt number correlations of the HHFs

Region	Ra number	C_1	C_2	C_3	C_4	C_5
1	<40,000	0.282	0.272	0.026	0.022	-0.082
2	40,000 – 4,000,000	0.337	0.252	0.076	0.025	-0.069

The form of correlations consist of several dimensionless parameter that affects the thermal behavior of HHF. The first part is $\left(\frac{D_o - D_i}{W}\right)$ that related to thickness effects. The second and the last parts are $\left(\frac{H}{D_o}\right)$ and $\left(\frac{D_i}{W}\right)$ that represent external and internal flows effects.

The comparison between the predicted Nusselt number correlations of HHFs and numerically-evaluated Nusselt number of HHF arrays is shown in Figure 22. It is found that the correlations have reasonable agreements with the numerical results with the average discrepancies of 3.0% for low Ra (Ra <40,000) and 2.7% for high Ra (40,000< Ra <4,000,000).

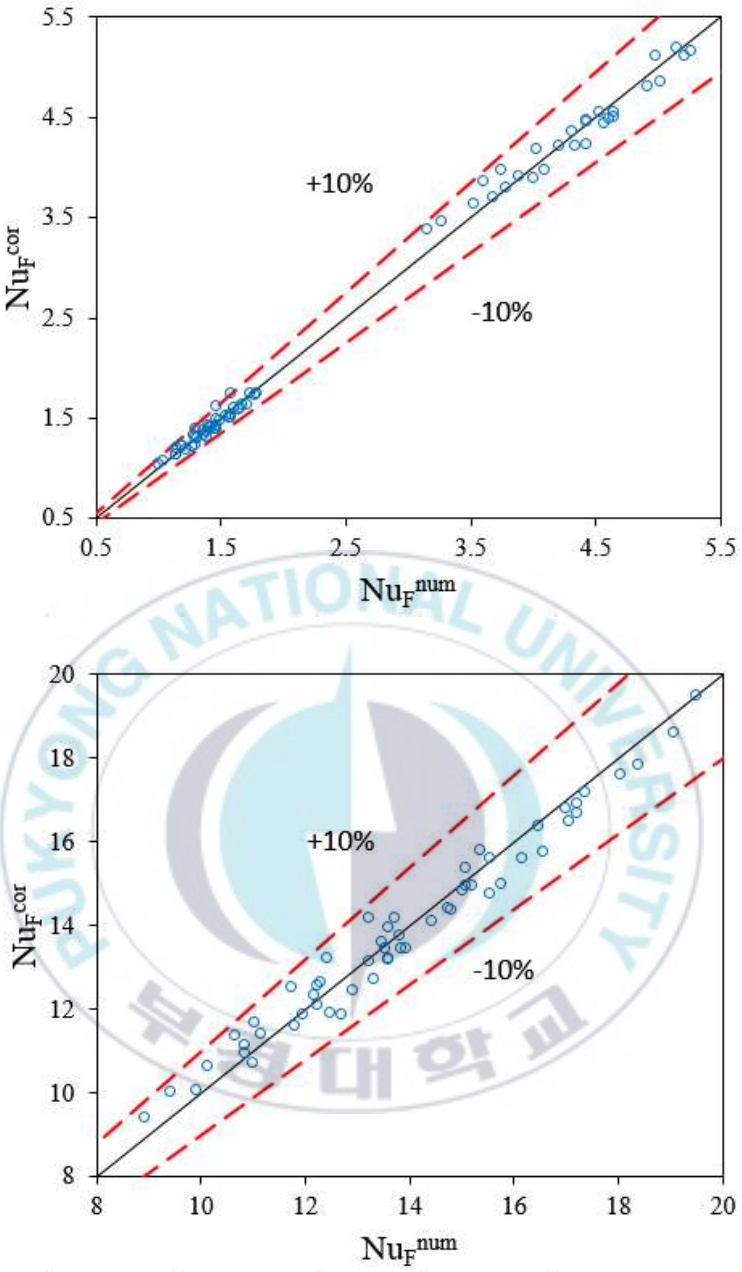

Figure 22. The predicted Nusselt number correlations of HHFs at (a) low Ra (b) high Ra as a function of numerically-evaluated Nusselt number of HHFs.

5.3.2 Nusselt Number of The HHF Array

Nusselt number and Rayleigh number of the HHF arrays is a function of fin spacing as a characteristic length and determined by considering the primary geometric parameters.

The correlation of Nusselt number of the HHF arrays was formulated as follows.

$$Nu_{FA}^{cor} = C_1 . \left(\frac{D_o - D_i}{H}\right)^{\left(\frac{H}{1000} - C_2\right)} (Ra_{FA})^{C_3} \left(\frac{S}{D_i}\right)^{C_4} \left(\frac{D_o}{D_o - D_i}\right)^{C_5} \quad (56)$$

where D_o is outer diameter, D_i is inner diameter, S is fin spacing, and H is height of the fin.

Several dimensionless parameters in the correlation represent important characteristic of the structure. The first is $\left(\frac{D_o - D_i}{H}\right)$ that related to fin efficiency. The second is $\left(\frac{S}{D_i}\right)$ that represents external and internal flows. The last dimensionless parameter is diameter effects, $\left(\frac{D_o}{D_o - D_i}\right)$, as a main parameter of the fin structure.

Nusselt number correlations of HHF arrays were defined for three regions of Rayleigh number, which are low range Ra (Ra <9000), midrange Ra (9000<Ra<60000), and high range Ra (60000<Ra <292000). The empirical constants of the fin arrays correlations are given in Table 11.

Table 11. Empirical constants of Nusselt number correlations of the HHF arrays

Region	Ra number	C_1	C_2	C_3	C_4	C_5
1	<9,000	0.000658	0.258	0.430	1.490	0.855
2	9,000-60,000	0.00169	0.231	0.156	1.601	1.877
3	60,000-292,000	0.00180	0.105	0.223	1.491	1.332

Figure 23 shows the predicted Nusselt number correlations of HHF arrays as a function of numerically-evaluated Nusselt number of HHF arrays. It is seen that the predicted Nusselt number correlations agrees well with numerically-evaluated Nusselt number. The average discrepancy values were 3.5% for Ra <9000, 8% for 9000<Ra<60000, and 2.8% for 60000<Ra <292000.

As has been noted, both of the predicted Nusselt number correlations of the HHFs and the HHF arrays have good agreements with the numerical data. Therefore, this could be considered that the correlations are vigorous to predict the thermal behaviors for natural convection around the HHFs and HHF array with upward face.

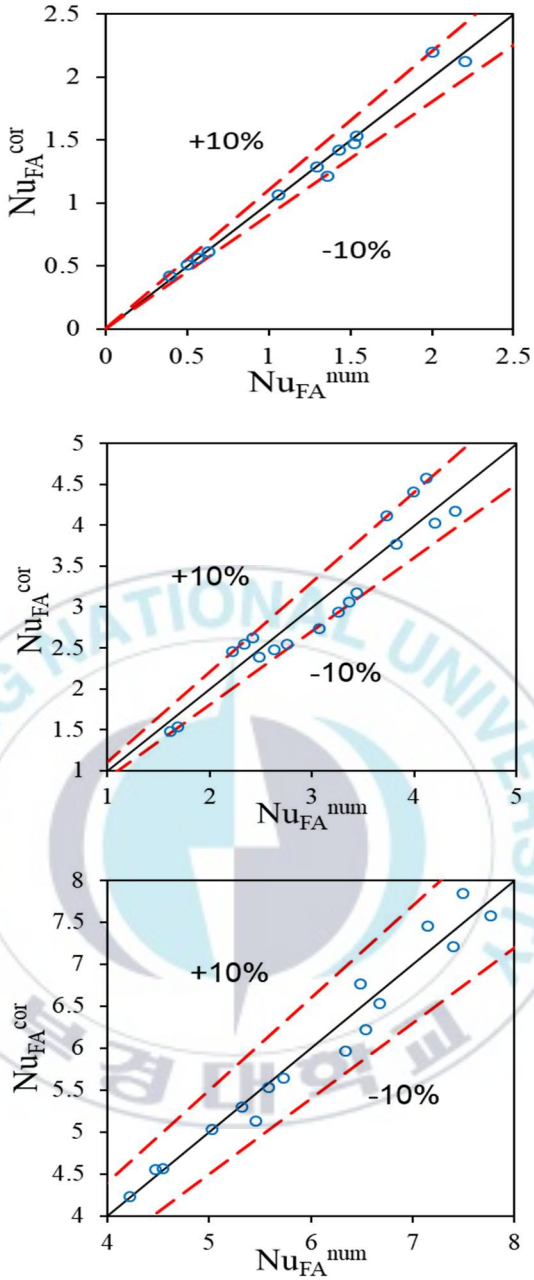

Figure 23. The predicted Nusselt number correlations of HHF arrays at (a) low Ra (b) medium Ra (c) high Ra as a function of numerically-evaluated Nusselt number of HHF arrays.

VI. Conclusions

The methodology to predict thermal behavior of the hollow hybrid fins (HHFs) and the HHF arrays under natural convection have been evaluated. HHF is a hollow pin fin integrated with radially-placed plate fins and having a perforation near the fin base. The HHF array is a staggered array of the HHFs. Wide-range CFD models were generated for both the HHFs and the HHF arrays. The 168 3D-models of HHFs and 48 3D-models of HHF arrays were numerically-calculated. The CFD models were validated with measurement results. The discrepancies between the numerical models and the measurements are lower than 10%.

The correlations of the HHFs and the HHF arrays have been developed. The HHF correlations were defined for two regions of Rayleigh number, which are low range Ra (Ra<40000) and high range Ra (40,000< Ra <4,000,000). The HHF arrays were defined for three regions of Rayleigh number, which are low range Ra (Ra <9000), midrange Ra (9000<Ra<60000), and high range Ra (60000<Ra <292000).

The results show that the prediction of both of the HHF correlations and the HHF array correlations agrees well with the CFD calculation with reasonable discrepancy. The average discrepancy values of HHF correlations were 3.0% for low range Ra (Ra<40000) and 2.7% for high range Ra (40,000< Ra <4,000,000). The average discrepancy values of HHF array correlations were 3.5% for Ra <9000,

8% for 9000<Ra<60000, and 2.8% for 60000<Ra <292000.

This research on the Nusselt number correlations developed for the HHFs and the fin arrays should be utilized to optimize structures of the HHFs and the arrays for developing high-performance lightweight heat sinks.

PUKYONG NATIONAL UNIVERSITY
부경대학교

List of Publications

1. N.S. Effendi, Sina Jamilah, Hyeon Ho Yang, Byoung Guk Kim, K.J. Kim, "Nusselt Number Correlation for Natural Convection Around Hollow Hybrid Fin", The Korean Society of Mechanical Engineers Proceedings, 2020.
2. Sina Jamilah, Hyeon Ho Yang, K.J. Kim, "Natural Convection Cooled Hollow Hybrid Fins", The Korean Society of Mechanical Engineers Proceedings, 2020.
3. Sina Jamilah, Hyeon Ho Yang, Wooheon Noh, K.J. Kim, "Nusselt Number Correlations for Natural Convection Hollow Hybrid Fins Arrays", The Korean Society of Mechanical Engineers Proceedings, 2021.
4. Sina Jamilah, Hyeon Ho Yang, Wooheon Noh, K.J. Kim, "Prediction Methods of Thermal Behaviors of Hollow Hybrid Fins and Fin Arrays under Natural Convection", The Korean Society of Mechanical Engineers Proceedings, 2021.
5. Sina Jamilah, Hyeon Ho Yang, Wooheon Noh, K.J. Kim, "Prediction Methods of Dimensional and Orientation Effects on Hollow Hybrid Fins and Fin Arrays under Natural Convection", in preparation.

PUKYONG NATIONAL UNIVERSITY 부경대학교

References

[1]. Moore, Arden L., Shi Li, 2014, “Emerging challenges and materials for thermal management of electronics”, Materials Today, Vo.17, No.4, pp.163-174.

[2]. Bloschock, Kristen P. and Bar-Cohen, A., 2012, “Advanced thermal management technologies for defense electronics”, Proc. Of SPIE, Vol.8405.

[3]. Ebrahimi, Khashayar., Ebrahimi, Sasan., Ebrahimi, Khosrow., 2020, “Fractal Pattern Effects on Natural Convection Heat Transfer and Flow Characteristics”, 19th IEEE ITHERM Conference.

[4]. Daniel A. Steigerwald, Jerome C. Bhat, Dave Collins, Robert M. Fletcher, Mari Ochiai Holcomb, Michael J. Ludowise, Paul S. Martin, and Serge L. Rudaz, 2002, “Illumination With Solid State Lighting Technology”, IEEE Journal, Vol.8, No.2, pp.310-320.

[5]. Schubert, E. F., Kim, J. K., 2005, “Solid-state light sources getting smart”, Science, 308, 1274-1278.

[6]. Arik, M., Petroski, J., Weaver, S., 2002, “Thermal challenges in the future generation solid state lighting applications: light emitting diodes”, 8th IEEE ITherm, 113-120.

[7]. Sonn, A. and Bar-Cohen,A., 1981, “Optimum cylindrical pin fin,” ASME J. Heat Transf., vol.103, pp. 814-815.

[8]. Bahadur, R. and Bar-Cohen, A., 2005, “Thermal design and optimization of

natural convection polymer pin fin heat sinks", IEEE Trans. on Compon. Packag. Technol., 28(2), 238-246.

[9]. Icoz, T. and Mehmet, M., 2010, "Light Weight High Performance Thermal Management with Advanced Heat Sinks and Extended Surfaces", IEEE Trans. on Compon. Packag. Technol., 33(1), pp.161-166.

[10]. Sparrow, E. M. and Vemuri, S. B., 1986, "Orientation Effects on Natural Convection/Radiation Heat Transfer from Pin-Fin Arrays", Int. J. of Heat Mass Transfer, 29(3), pp. 359-368.

[11]. Jang, D., Kim, D-R., Lee, K.-S., 2015, "Correlation of cross-cut cylindrical heat sink to improve the orientation effect of LED light bulbs", Int. J. Heat Mass Transfer, 84, pp. 821-826.

[12]. Sertkaya, A. A., Bilir, S., Kargici, S., 2011, "Experimental Investigation of the Effects of Orientation Angle on Heat Transfer Performance of Pin-Finned Surfaces in Natural Convection", Energy, 36, pp. 1513-1517.

[13]. Huang, R.-T., Sheu, W.-J., Wang, C.-C., 2008, "Orientation Effect on Natural Convective Performance of Square Pin Fin Heat Sinks", Int. J. of Heat Mass Transfer, 51(9), pp. 2368-2376.

[14]. Shen, Q., Sun, D., Xu, Y., Jin, T., Zhao, X., 2014, "Orientation Effects on Natural Convection Heat Dissipation of Rectangular Fin Heat Sinks Mounted on LEDs", Int. J. of Heat Mass Transfer, 75, pp. 462-469.

[15]. Aihara, T., Maruyama, S., Kobayakawa, S., 1990, "Free convective/radiative heat transfer from pin-fin arrays with a vertical base plate (general

representation of heat transfer performance)", Int. J. Heat Mass Transfer, 33, pp. 1223-1232.

[16]. Elshafei, E.A.M., 2010, "Natural Convection Heat Transfer from a Heat Sink with Hollow/Perforated Circular Pin Fins", Energy, 35(7), pp. 2870-2877.

[17]. Jang, D., Yu, S.-H., Lee, K.-S., 2012, "Multidisplinary Optimization of a Pin-Fin Radial Heat Sink for LED Lighting Applications", Int. J. of Heat Mass Transfer, 55, pp. 515-521.

[18]. Kou, H.S., Lee, J.J., and Chen, C.W., 2008, "Optimum Thermal Analysis of a Heat Sink with Various Cross-Sections by Adjusting Fin Length and Cross-Section", Heat Transfer Eng, 29(6), pp. 537-545.

[19]. Kim, H., Kim, K.J., and Lee, Y. W., 2012, "Thermal performance of smart heat sinks for cooling high power LED modules", 13th IEEE Intersociety Conference on Thermal and Thermomechanical Phenomena in Electronic Systems, 62-67.

[20]. Kim, K. J., 2013, "Performance of hybrid fin heat sinks for thermal control of light emitting diode lighting modules", Journal of Electronic Packaging, 136(1), 011002.

[21]. Kim, K.J., 2014, "Orientation effects on the performance of natural convection cooled hybrid fins", 20th International Workshop on Thermal Investigations of ICs and Systems, Greenwich, UK, 1-3.

[22]. Effendi, N. S., Kim, K. J., 2015, "Thermal behaviors of passively cooled

hybrid fin heat sinks for lightweight and high performance thermal management", the ASME 2015 InterPACKICNMM, San Francisco, USA, V001T09A005.

[23]. N. S. Effendi and K. J. Kim, 2017, "Orientation effects on natural convective performance of hybrid fin heat sinks", J. Applied Thermal Engineering, vol. 132, pp.527-536.

[24]. N. S. Effendi and K. J. Kim, 2018, "Natural convective hybrid fin heat sinks for lightweight and high performance thermal management", J. Mech. Sci. Technol., vol. 32, no. 10, pp. 5005–5013.

[25]. N. S. Effendi, S. S. G. R. Putra, and K. J. Kim, 2018, "Prediction methods for natural convection around hollow hybrid fin heat sinks" International Journal of Thermal Science, 126, pp. 272-280.

[26]. S. S. G. R. Putra, N. S. Effendi, and K. J. Kim, 2019, "A parametric study on structural effects of hollow hybrid fin heat sinks in natural convection and radiation", J. Mech. Sci. Technol., vol. 33, no. 6, pp. 2985–2993.

[27]. K. A Hoffmann and S. T. Chiang, 1998, "Computational fluid dynamics" Volume I, 3rd Ed., Engineering Education System, Wichita, KS.

[28]. ANSYS, Inc., ANSYS FLUENT: User's guide, Canonsburg, PA, 2016

[29]. K.S. Al-Athel, 2017, "A computational methodology for assessing the thermal behavior of metal foam heat sinks", Applied Thermal Engineering 111, pp.884-893.

[30]. J. Taylor, 1997, "An introduction to error analysis, the study of uncertainties

in physical measurements", Second ed., University Science Books, Sausalito, CA.

[31]. R. J. Moffat, 1988, "Describing the Uncertainties in Experimental Results", Experimental Thermal and Fluid Science, 1:3-17.

[32]. D. F. Young, B. R. Munson, T. H. Okiishi and W. W. Huebsch, 2010, "A Brief
Introduction to Fluid Mechanics", John Wiley & Sons.

[33]. F. P. Incropera, D. P. DeWitt, T. L. Bergam, A. S. Lavine, 2006, "Fundamentals of heat and mass transfer", Sixth edition, John Wiley & Sons.

PUKYONG NATIONAL UNIVERSITY
부경대학교